DOI: 10.1002/ejic.200800130

Polymer-Mediated Growth of Highly Crystalline Nano- and Micro-Sized $LiNi_{0.5}Mn_{1.5}O_4$ Spinels

José Carlos Arrebola,[a] Alvaro Caballero,[a] Lourdes Hernán,*[a] and Julián Morales[a]

Keywords: Crystal growth / Polymers / Spinel phases / Lithium batteries

The use of polymers containing oxygen-based functional groups [polyethylene glycol (PEG), poly(methyl methacrylate) (PMMA)] has been studied to synthesize highly crystalline nanometric $LiNi_{0.5}Mn_{1.5}O_4$ spinel. Polyvinylidene fluoride (PVDF), which was also tested, failed in the spinel synthesis. Mechanical activation of hydrated salts in the presence of oxalic acid and the polymer, followed by heating at 800 °C for a few minutes, is sufficient to obtain pseudopolyhedral particles ranging from 60–80 nm in size. X-ray broadening analysis and the electron micrographs of the microstructure reveal that the polymer has an improved particle crystallinity. Calcining at 400 °C tailors the particle shape towards a nanorod-like morphology due to the nonionic surfactant properties of PEG. The ability of the functional groups of these polymers to bind to metal ions brings them closer and therefore shortens the diffusion paths followed to adopt the spinel structure. At high temperature, the particles adopt a well-defined pseudopolyhedral morphology with a smooth texture and a lower microstrain content than that obtained in the absence of polymer. The results of the electrochemical tests show that the polymer-assisted nanoparticles exhibit improved reversible capacity and better cycling properties as electrode materials in lithium cells. The improved crystallinity of the particles is the key factor in this respect, particularly when the cells are operated at low rates.

Introduction

The spinel framework is a well-known structure that is adopted by a large numbers of compounds and particularly transition metal-based oxides, which exhibit salient electronic properties of the electric, magnetic and catalytic type.[1] Li-containing spinels, particularly $LiMn_2O_4$,[2] have received special attention in the last decade as this spinel has the ability to reversibly extract and insert lithium and has been proposed as an alternative to $LiCoO_2$, which is used as the cathode material in commercial batteries but is more toxic and expensive than the spinel. Replacing Mn with other transition metals such as Ni not only results in improved stability on cycling but also provides an interesting electrochemical property, namely an expanded voltage window spanning up to 5.0 V vs. the lithium electrode.[3,4] $LiNi_{0.5}Mn_{1.5}O_4$ spinel is the best replacement candidate[5] as it has the ability to reversibly extract and insert lithium at 4.6–4.8 V on prolonged cycling[6–9] and delivers the highest possible capacity. This can open up new prospects for a novel generation of lithium-ion batteries with a higher specific energy, which is especially interesting with a view to their use as power sources in hybrid vehicles. However, this attractive property must be also accompanied by a high power density, a condition that is usually not attainable due to extensive polarization at high charge-discharge rates.[10] This increased polarization has been ascribed to slow lithium diffusion in the solid active materials.

The use of particles with sizes in the nanometric range (below 100 nm) can alleviate this shortcoming due to a shortening of the displacement distance for lithium ions.[11,12] Furthermore, the high surface area of these materials can facilitate the diffusion of lithium ions in the sample and improve the rate capability of the compound.[13] However, the reactivity towards lithium is influenced by both particle size and other properties such as particle shape and the degree of crystallinity and agglomeration. Because these properties are strongly affected by the synthetic conditions, the search for methods capable of tailoring all these variables is a current research field. In this context, the use of polymers in the synthesis of spinels is an effective strategy for modifying their textural properties.[14] Indeed, unusual particle morphologies have been observed due to the effect of polymers facilitating particle growth in specific directions.[15–17] In this work, we examine the influence of two different polymers, namely polyethylene glycol (PEG) and poly(methyl methacrylate) (PMMA) on the synthesis of $LiNi_{0.5}Mn_{1.5}O_4$. These polymers have different functional groups that can result in differences in the formation of nuclei and the direction in which crystals grow. For com-

[a] Departamento de Química Inorgánica e Ingeniería Química, Edificio Marie Curie, Campus de Rabanales, Universidad de Córdoba,
14071 Córdoba, Spain
E-mail: iq1hepal@uco.es

Supporting information for this article is available on the WWW under http://www.eurjic.org or from the author.

parison, the spinel was also synthesized in the absence of polymer. The synthetic methods used resulted in significant differences in particle morphology, size and crystallinity. Consequently, the performance of electrodes made from these spinels is clearly influenced by their synthetic conditions. Thus, the particles prepared using the polymer-assisted method exhibit improved cycling reversibility and capacity relative to the spinel obtained in the absence of polymer.

Results and Discussion

Structural and Morphological Characterization

The synthesis of the spinels involves two steps: (1) mechanochemical treatment at ambient temperature to convert acetates into nanometric oxalates[18,19] (oxalic acid is stronger and less volatile than acetic acid and oxalate ions are excellent ligands for transition metal ions), and (2) thermal decomposition of nanometric oxalates and polymer pyrolysis to obtain the spinel phase.[20] This latter process can be followed by TG measurements combined with analysis of the gases evolved by mass spectrometry, as shown in Figure 1. We only monitored the species H_2O and CO_2 since no other gases that might be formed (e.g. CO, the molecular weight of which is identical to that of N_2) could be identified. The main weight loss occurs below 450 °C, where the spinel is already formed, irrespective of the specific synthetic conditions used. However, the presence of the polymer caused other alterations that are worth noting. For example, the weight loss of the mixture without polymer occurred in two steps spanning the ranges 150–250 and 350–420 °C. Water was evolved in the first step and the weight loss of around 20% is close to the amount of water assigned to oxalic acid. The detection of CO_2 above 350 °C, where the second step was found to occur, is consistent with oxalate decomposition; the resulting weight loss (ca. 40%) is reasonably consistent with that calculated from the conversion of precursor acetates into oxalates (44%).

The presence of polymer, whatever its nature, appears to have little effect on the decomposition temperature of oxalates. Moreover, polymer degradation occurs at temperatures above that of the oxalate and somewhat higher than that of the pure polymer (the TG curve for PEG1500 has been included for comparison), as shown by the slope change in the TG curve and, particularly, by the release of CO_2 and H_2O in the higher temperature range. We ascribed the formation of CO_2 to the presence of traces of oxygen in the carrier gas. The CO_2 signal for the PEG composite is split into two peaks, with the temperature of the lower-intensity peak coinciding with that observed for the mixture without polymer. The thermal decomposition of PMMA is somewhat more complex as CO_2 is released in two steps. The shoulder on the left-hand side of the signal might be due to CO_2 from the oxalate component. The presence of carbonyl and carboxyl groups may account for this result. The weight loss assigned to polymer pyrolysis (around 20%) is consistent with the amount of polymer added. The degree

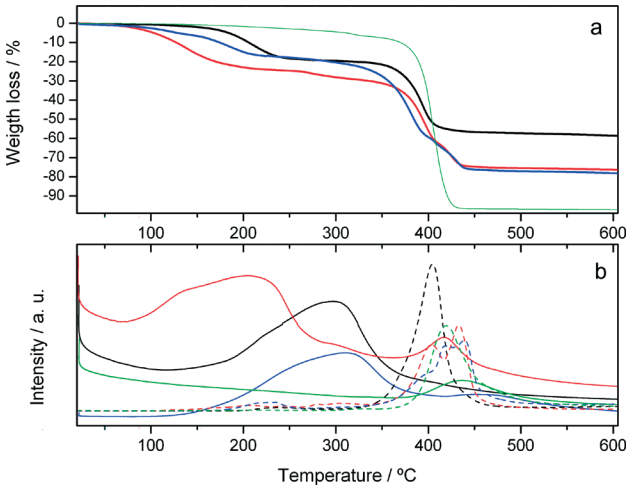

Figure 1. (a) TG curves for the precursors without polymer (black line), with PEG 1500 (red line), PMMA (blue line) and polymer PEG1500 (green line). (b) Evolution of H_2O (solid line) and CO_2 (dash line).

of hydration of the polymer-containing samples (particularly the PEG sample) is somewhat higher, possibly as a result of the morphological and mechanical properties of the polymer hindering the release of heat produced during the grinding process and of the sample retaining an increased amount of water.

Figure 2 shows the X-ray powder diffraction patterns for some spinels. All lines can be indexed to the spinel structure, thus indicating a high degree of purity. Some minor peaks due to impurities can be seen for the samples calcined at 400 °C (Figure 2, a). These peaks (labeled with *) are assigned to NiO, which is commonly detected in the synthesis of this spinel using conventional ceramic methods,[21] and disappear on increasing the calcination temperature. Different heating temperatures resulted in subtle differences. Thus, the diffraction peaks obtained at 400 °C were weaker and broader, which suggests lower crystallinity, whereas those obtained at 800 °C were stronger and

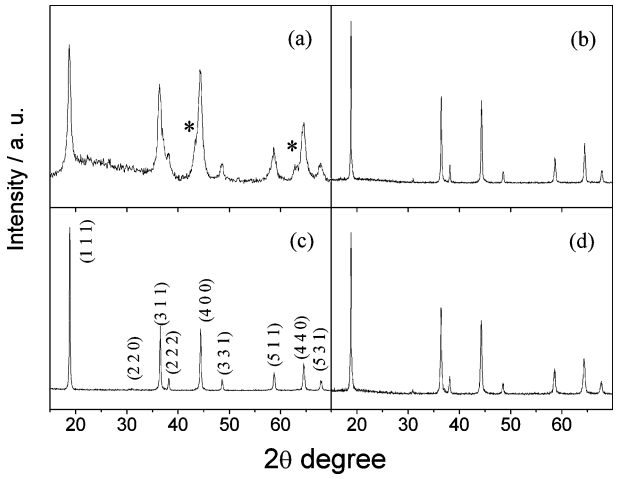

Figure 2. XRD patterns for the Li-Ni-Mn spinels: (a) PEG-400, (b) S-800, (c) PEG-800 and (d) PMMA-800.

sharper. The lattice parameters obtained are shown in Table 1. The average value of around 8.18 Å is consistent with previously reported values for spinels with a similar composition.[22]

Table 1. Unit cell dimensions, specific surface area, crystallite size and microstrain contents of $LiNi_{0.5}Mn_{1.5}O_4$ spinels.

Sample	a [Å]	S_{BET} [$m^2 g^{-1}$]	D[a] [nm]	D[b] [nm]	Microstrains ($\times 10^{-3}$)
S-800	8.178	12	66	139	1.90
S-800–5	8.188	6	98	367	1.51
PEG-400	8.184	67	–	–	–
PEG-800	8.173	16	62	84	1.50
PEG-800–5	8.178	5	130	270	0.85
PMMA-800	8.181	9	79	107	1.03
PMMA-800-5	8.188	4	161	125	0.30

[a] Values obtained from the Scherrer equation. [b] Williamson and Hall equation.

The microstructure of the bulk spinels was evaluated from the full width at half maximum of the diffraction lines, which provides information on the mean crystallite size (size of the coherent crystalline domain); lattice imperfections (microstrains) were evaluated from the degree of XRD line broadening. The Williamson–Hall equation [see Equation (1)] was used to determine these two parameters.[23]

$$\beta \cos\theta = 2<e> \operatorname{sen}\theta + 0.9\lambda/D \quad (1)$$

where β is the integral breadth after correction for instrumental broadening from highly crystalline quartz and kα_2 elimination using the Rachinger method,[24] $<e>$ denotes local strains (defined as $\Delta d/d$, where d is the interplanar space) and D is crystallite size. Equation (1) was applied to the four strongest reflections [viz. (111), (331), (511) and (531)] as they do not overlap with any other reflection. Furthermore, the equation was only applied to the samples prepared at 800 °C as those obtained at 400 °C had a high signal-to-noise ratio and precluded accurate measurements of the full-width at half-maximum (FWHM). Figure S1 in the Supporting Information shows the plots of the above equation for selected spinels and Table 1 lists the crystallite sizes and strains calculated from the intercepts and slopes, respectively. As expected, the crystallite size increases and the microstrain content decreases with heating time, which reflects improved crystallinity in the spinel.[25] Furthermore, under identical synthetic conditions, the presence of polymer improves particle crystallinity as the microstrain content decreases under these conditions.

Figure 3 shows TEM images for the three spinels calcined at 800 °C for 5 min. The particle size is below 100 nm in all cases and the presence of polymer clearly influences the particle shape. Thus, the absence of polymer results in nanoparticles with an ill-defined shape and a strong tendency to agglomerate, which is typical of nanometric materials. In the presence of polymer, however, the particles adopt a more regular, pseudo-polyhedral morphology typical of spinels.[26] The particle sizes are approximately 60 or 80 nm for PEG and PMMA, respectively, which is somewhat lower than the crystallite size obtained from Equation (1). A better agreement was obtained when the crystallite size was calculated from the Scherrer equation[23] (higher for PMMA-800), which gave a value more consistent with the specific surface values (lower for PMMA-800; see Table 1). These differences are more apparent in the images obtained at higher resolutions, where the polyhedral shape, with well-defined edges and corners, becomes clearly visible (Figure 3, d). The HREM images (Figure 3, e) reveal a high crystallinity and the apparent absence of imperfections. The interplanar spacing was calculated to be around 0.45 nm, which corresponds to the orientation of the (111) atomic planes. Small particles with a low defect content are quite amenable to cycling at high charge/discharge rates as the displacement of Li ions is favored by the decreased probability of meeting with defects that might truncate their movements. S-800 particles, in contrast, exhibit ill-defined edges and a rougher surface (see Figure 3, f). However, this compound also exhibits ordered (111) planes, which is consistent with the XRD pattern (Figure 2, b), and a well-developed spinel structure.

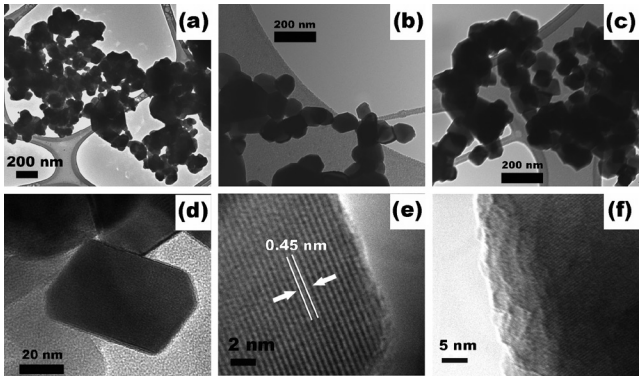

Figure 3. TEM images of the spinels: (a) S-800, (b) PEG-800, (c) PMMA-800. Images recorded at higher magnifications: (d) and (e) PMMA-800; (f) S-800.

Surfactants are known to effectively tailor particle shape and size in synthetic processes, and various nanostructured spinels (particularly spinel-type ferrites) have been synthesized in the form of nanorods,[27] nanowires[28] and nanotubes[29] by using a template method. PEG is a good dispersant, nonionic surfactant polymer with a long zigzag chain that can facilitate particle growth in certain directions, whereas PMMA is a rigid polymer that possesses methyl groups which act as hooks and hinder chain slippage. As stated above, two features become apparent at temperatures as low as 400 °C: 1) the spinel framework is already formed and 2) the organic network, the main components of which are the oxalate precursor and the polymer, is virtually lost. Figure 4 (a) shows a TEM image of the sample PEG-400 corresponding to the spinel synthesized at 400 °C in the presence of PEG. The particles are nanorod-like in shape, several hundreds of nanometers long and 40–60 nm wide. Longer and narrower particles with a nanorod-like morphology have also been obtained using PEG 400.[8] These nanorods consist of nanograins with a pseudohexagonal shape that are quite uniform in size (approx. 10 nm, as re-

vealed by the HREM image in Figure 4, b). Their crystalline nature is supported by the interplanar spacing, as evaluated from the fringes. This image also shows that nanorods are formed by randomly oriented spinel nanocrystals. Thus, the nanorod-like morphology must be due to the presence of a thin layer of undecomposed polymer acting as binder and preventing dispersion of nanocrystals. This texture is consistent with the high value of the specific surface area and the hysteresis loop observed in the adsorption/desorption nitrogen isotherms (see Figure S2 in the Supporting Information), which were assigned to a mesoporous system with pores of around 8 nm on average.

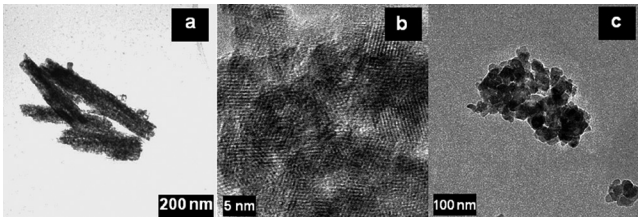

Figure 4. TEM images of the spinels calcined at 400 °C for 5 min. Samples prepared with PEG-1500 [(a) and (b)] and PMMA (c).

The previous results strongly support the assumption that the polymer forms a barrier that hinders particle growth. Surfactants (e.g. polymers) are known to adsorb to the surfaces of growing particles and create a shield against van der Waals interactions between particles, thus inhibiting particle aggregation. Under these conditions, sintering is hindered and the nanometric size is enhanced. PEG can be absorbed on the surfaces of oxide nuclei and modify their growth kinetics and favor anisotropic growth of crystals as a result. PEG chains bind to the surface of oxide nuclei and nanoparticles through either hydrogen bonds formed by hydroxy groups or, more probably, through interactions between oxygen-functionalized groups in the polymer and metal ions in the spinel precursor. The flexible properties of this polymer allow the spinel particle shape to be tailored to a nanorod-like morphology. Figure 5 illustrates the formation of particles synthesized in the presence of PEG. The process is based on the chemical adsorption of metal oxalates onto the polymer surface,[30] with the polymer morphology being retained after the organic substances are removed by calcination. In contrast, the spinel prepared at 400 °C in the presence of PMMA adopts no special morphology and the nanoparticles form agglomerates (see Figure 4, c). The rigid framework of the polymer,

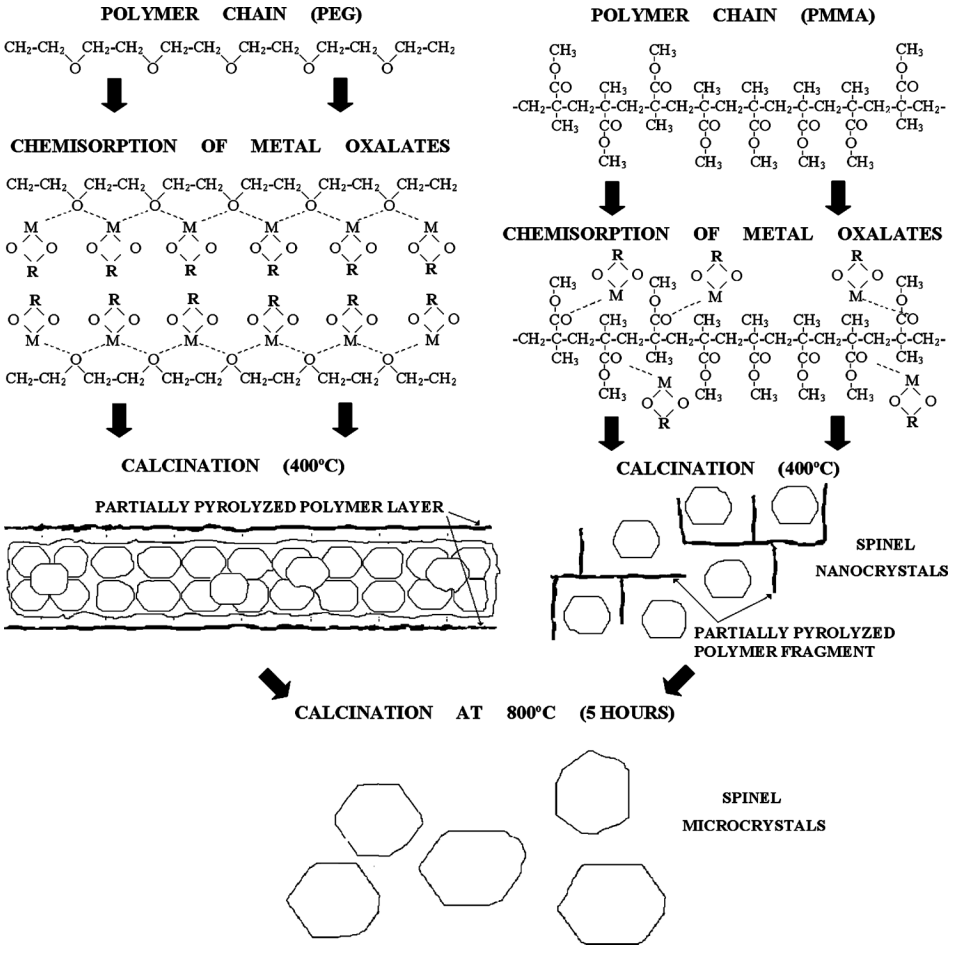

Figure 5. Representative illustration of a Li-Ni-Mn spinel synthesis in the presence of polymer.

the random orientation of the functional groups and probably also the stronger interaction of the carbonyl group with the precursor cations facilitate the fragmentation of the polymer and preclude retention of the polymer morphology after calcination. As a result, growth of the spinel in a nanorod-like morphology is hindered and the particles do not exhibit a special orientation (Figure 5).

The proposed model was supported by the IR spectra, which exhibit shifts in the peaks assigned to the oxygen-based functional groups in the polymer. Figure 6 shows the IR spectra for PEG1500 and PMMA, and also those for their ground mixtures with inorganic precursors following further calcining at 400 °C, which caused the polymers to partially decompose (see Figure 1, a). In order to simplify the description of the IR spectra, we have focused on the ν_{C-O-C} (1105 cm^{-1}) and $\nu_{C=O}$ (1731 cm^{-1}) vibrations for PEG1500 and PMMA, respectively, as these groups have the ability to coordinate to metal ions. No other peaks assigned to the precursors (mainly those for oxalates) are present in the vibrational region of the ether group. The peak assigned to this group decreases in intensity on heating at 400 °C. Under these conditions, it becomes a very weak, broad signal shifted to a somewhat lower wavenumber (1088 cm^{-1}). This shift to lower energy may be consistent with a weak interaction of the ether group with the metals. As expected, the greater similarity between the functional groups of PMMA and precursors is apparent from the spectra shown in Figure 6 (b), where the bands for their carbonyl groups appear at 1731 and approximately 1650 cm^{-1}, respectively. The low frequency of oxalate compared to PMMA can be ascribed to a combination of the resonance of the carboxyl group and its binding to the metal ions. The most salient effect of heating is the disappearance of the polymer peak in spite of the relatively low calcination temperature used (below that needed for complete removal of the polymer, but above the decomposition temperature for the oxalate components, see Figure 1). We believe that part of the polymer remains undecomposed even though its carbonyl stretching frequency decreases upon binding of the metal ions[31] and the peak is superimposed on that for oxalate ion. On the other hand, the greater frequency decrease observed in the PMMA system relative to PEG is consistent with a stronger interaction of the former polymer with the precursor cations through the carbonyl groups. The increased decomposition temperatures of the polymers in the composites relative to the pure polymers (see parts a and b of Figure 1) could be a result of such metal–polymer interactions.

A second effect promoted by the presence of the two polymers used in the synthetic procedure is improved spinel crystallinity. This seems to be independent of the surface properties of the polymer, the role of which must be related to its ability to coordinate to the metal ions forming the spinel. As stated above, the functional groups of the polymer capable of acting as basic Lewis sites might bind to the ions, thus shortening their diffusion paths to adopt the spinel structure. This model is consistent with the results obtained by using a polymer such as polyvinylidene fluoride

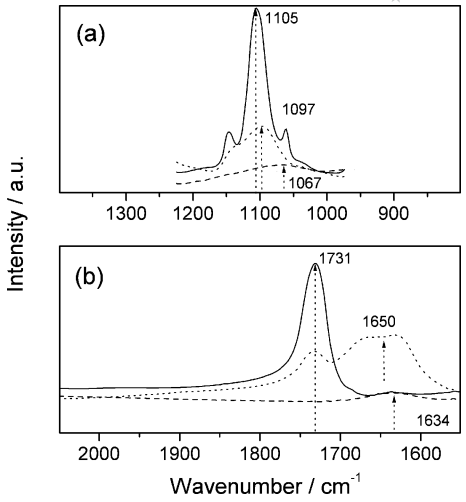

Figure 6. FTIR spectra for the PEG-1500 (a) and PMMA (b) systems (only the region corresponding to ν_{C-O-C} and $\nu_{C=O}$ vibrations): pure polymer (solid line), polymer–precursor mixture (dotted line) and mixture calcined at 400 C (dashed line).

(PVDF), which contains no functional oxygen atoms. In fact, this polymer is known to be an effective fluorinating agent.[32] In this case, the spinel synthesis failed, which suggests that the functional groups of the polymer must be a key factor for the spinel synthesis and might be able to approach and stabilize the metal ions by chelation.

The influence of the heating time on particle morphology was studied at a fixed temperature of 800 °C. Similar results were obtained with both polymers, so the following discussion refers to PMMA alone. Parts a and b of Figure 7 show SEM images of samples PMMA-800-5 and S-800-5, which were calcined for 5 h. The particles obtained in the presence of polymer are much bigger (average size 1 μm) but retain the polyhedral morphology of the nanometric particles. As expected, this increase in particle size results in a decrease in the specific surface area to 3.7 $m^2 g^{-1}$ (see Table 1). Increasing the heating time to 24 h hardly alters the particle size or specific surface area, which suggests that sintering at this temperature reaches a critical size of about 1 μm. Longer heating times reduce the particle contact and slow kinetic growth. Increasing the particle size therefore entails raising the heating temperature.

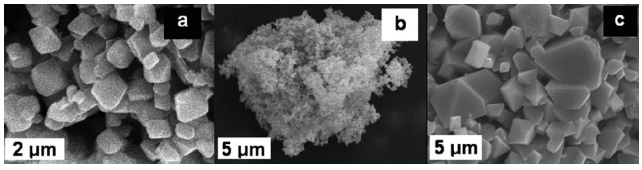

Figure 7. SEM images of the spinels: (a) PMMA-800-5, (b) S-800-5. (c) The latter sample heated at 900 °C for 48 h.

The particles calcined in the absence of PMMA exhibit quite a different morphology (Figure 7, b). Thus, they are irregular in shape and size and tend to agglomerate. Improving the crystallinity therefore requires using higher

temperatures (900 °C) and a longer time (48 h). Under these conditions, pseudo-octahedral particles with a size of around 5 μm were obtained (Figure 7, c).

Electrochemical Properties

The spinels were tested as electrodes for lithium-ion batteries. For this purpose, we chose the spinels calcined at 800 °C as highly defective materials are well known to exhibit a poor electrochemical performance in such devices.[33] This shortcoming affects the spinels prepared at 400 °C, as shown by the high signal-to-noise ratio of the XRD patterns and the broad diffraction peaks obtained (see Figure 2). The cells were studied at two charge/discharge rates, namely C/4 and 2C (C represents 1 Li^+ ion exchanged in 1 h, equivalent to 148 mA g^{-1}). In general, the nanometric particles exhibit a good performance at high rates due to the shortened diffusion paths, whereas at low rates the increased reactivity towards the electrolyte prevails and lowers the cell performance. Micrometric particles, which are less reactive towards the electrolyte, are a better choice for making electrodes under these latter conditions.

Figure 8 (a, b) show the second charge and discharge curves for the different spinels recorded at C/4. The first charge curve for this spinel is affected by various factors (viz. formation of a solid electrolyte interface accompanied by electrolyte decomposition[34] and release of oxygen from the spinel lattice[35]), which results in substantial overcharge. For this reason, the first cycle was disregarded and the following comments focus on the second. The shape of these curves is typical for $LiNi_{0.5}Mn_{1.5}O_4$ spinel. Thus, the charge curves exhibit two regions of electrochemical activity over the ranges 3.9–4.4 and 4.5–5.0 V, respectively. The pseudo-plateau observed in the low voltage region is related to the Mn^{3+}/Mn^{4+} redox couple and its length is somewhat greater for the sample prepared with PMMA. We assign the presence of a small amount of Mn^{3+} due to the formation of some Ni^{3+}, as identified by XPS.[36,37] Electrochemical activity occurs mainly in the 4.7–5.0 V region, where a double pseudo-plateau associated with the $Ni^{2+} \rightarrow Ni^{4+}$ process, the mechanism of which reportedly involves two cubic/cubic two-phase reactions,[38] appears. Based on spectroscopic results,[39] the oxidation of Ni^{2+} to Ni^{4+} takes place via the following reactions involving the formation of Ni^{3+} as an intermediate species, see Equation (2).

$$Li[Ni^{2+}_{0.5}Mn^{4+}_{1.5}]O_4 \rightarrow Li_{0.5}[Ni^{3+}_{0.5}Mn^{4+}_{1.5}]O_4 + 0.5\ Li^+ + 0.5\ e^- \rightarrow [Ni^{4+}_{0.5}Mn^{4+}_{1.5}]O_4 + 0.5\ Li^+ + 0.5\ e^- \quad (2)$$

The discharge curves also exhibit two regions of electrochemical activity, thus indicating that the processes undergone by the spinel during charging of the cell are reversible. The capacity delivered by the cell was higher for the spinel prepared in the presence of polymer. The values range from 130 mAh g^{-1} for the spinel prepared with PMMA to 110 mAh g^{-1} in the absence of polymer. These values are 13% and 25% lower, respectively, than calculated for a stoichiometric spinel. The capacity values delivered by the cells on further cycling (Figure 9) basically retain the same features observed in the second cycle, namely a higher capacity in the cell made from the spinel synthesized in the presence of polymer. However, there are some differences worthy of comment. Thus, the PMMA-800-5 spinel delivers the highest capacity at C/4 (Figure 9, a). This is consistent with its higher crystallite size (also reflected in lowest specific surface area, Table 1) and lower microstrain content, both of which are consistent with its higher crystallinity. The electrochemical responses of the S-, PEG- and PMMA-800 samples are virtually identical, with the spinels synthesized in the presence of polymer delivering higher capacity values (Figure 9, b). However, the differences between PEG- and PMMA-800 spinels are more subtle and are consistent with a greater resemblance between their textural and microstructural properties. An interesting feature was observed at 2C. With nanometric particles (viz. the three spinels heated at 800 °C for 5 min; Figure 9, c), the cells delivering the highest capacity values are those made from the spinels prepared in the presence of polymer, which exhibit the best crystallinity-related parameters (viz. higher crystallite sizes

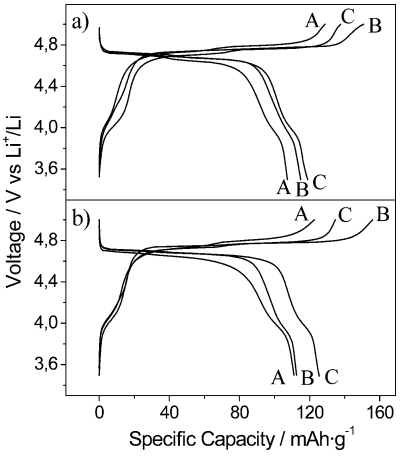

Figure 8. Second charge-discharge curve for Li/Li-M-Mn-O cells recorded over the voltage range 3.5–5.0 V. Spinels calcined at 800 °C for 5 min (a) and 5 h (b). Samples prepared in the absence of polymer (A), with PEG-1500 (B) and with PMMA (C).

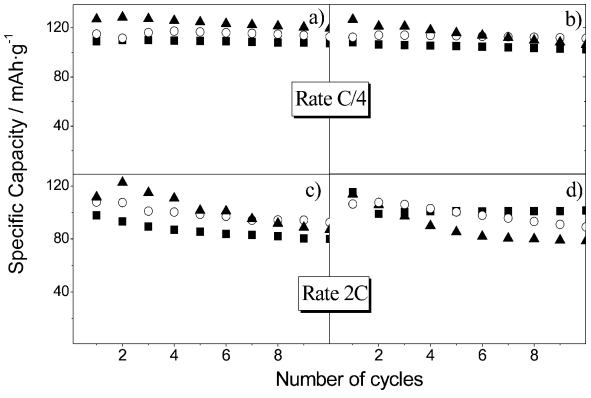

Figure 9. Variation of the specific capacity of Li/Li-M-Mn-O cells cycled over the voltage range 3.5–5.0 V. Samples calcined at 800 °C for 5 h [(a), (d)] and 5 min [(b), (c)]. Samples prepared in absence of polymer (■) and with PEG-1500 (○) and PMMA (▲).

and lower microstrain contents). In contrast, for the spinels calcined at 800 °C for 5 h (Figure 9, d), the cell made from the spinel prepared in the absence of polymer delivers higher capacity values after the first few cycles. This is consistent with the increased particle size of the spinel synthesized in the presence of polymer. Under these conditions, these spinels become micrometric in size, whereas S-800-5 particles remain nanometric.

Conclusions

The use of polymers containing oxygen-based functional groups (e.g., PEG, PMMA) in the synthesis of $LiNi_{0.5}Mn_{1.5}O_4$ spinel favors the formation of nanoparticles with high crystallinity. The ability of these functional groups to bind to metal ions in the spinel brings them closer together and shortens the diffusion paths for oxides to form. The particles adopt a well-defined pseudopolyhedral morphology with a smooth texture and a lower microstrain content than those obtained in the absence of polymer. The results of the electrochemical tests show that the polymer-assisted nanoparticles exhibit improved reversible capacity and better cycling properties as electrode materials in lithium cells. We believe that the improved electrochemical performance of the spinel is the combined result of its nanometric size and high crystallinity.

Experimental Section

General: All chemical used were analytical grade and were obtained from Sigma–Aldrich. The different spinels were prepared from identical precursors, namely $LiOAc{\cdot}H_2O$, $MnOAc_2{\cdot}4H_2O$ and $NiOAc_2{\cdot}2H_2O$ mixed in stoichiometric proportions with $H_2C_2O_4{\cdot}2H_2O$. A planetary Restach ball mill furnished with agate balls and an agate jar was used to obtain homogeneous mixtures formed from about 5 g of mixed precursors and 2.5 g of the acid. In a second step, 2.5 g of polymer (PEG-1500, PMMA and PVDF) was added and grinding continued for 60 min. The product thus obtained was a green solid which was calcined at 400 or 800 °C. All heating treatments were carried out under ambient conditions. Two samples (S-800, S-800-5) were obtained in the absence of polymer by heating the mixtures to 800 °C at 10 °C min^{-1} for 5 min and 5 h, respectively. Three samples were obtained from PEG1500, one by heating to 400 °C at 1 °C min^{-1} for 5 min (PEG-400) and the other two (PEG-800 and PEG-800-5) by using the same experimental conditions as for the samples obtained in the absence of polymer. These latter conditions (viz. heating at 800 °C for 5 min or 5 h) were also used to prepare the spinel in the presence of PMMA (samples PMMA-800 and PMMA-800-5).

X-ray diffraction (XRD) patterns were recorded with a Siemens D5000 X-ray diffractometer using non-monochromated Cu-K_α radiation and a graphite monochromator for the diffracted beam. Thermogravimetric measurements were performed with a Setsys Evolution 16/18 instrument from Setaram at a heating rate of 10 °C min^{-1} under a dynamic N_2 atmosphere (flow rate 20 mL min^{-1}). Mass spectrometric analysis of the gases evolved during thermal decomposition − only the signals for water and carbon dioxide were monitored − was performed with an EM-Pfeiffer Vacuum Omnistar instrument. Transmission electron microscopy (TEM) images were obtained with a Phillips TEM instrument operating at 100 keV and SEM images with a Jeol 6400 scanning electron microscope. Specific surface areas were determined with a Micromeritics ASAP 2000 instrument using N_2 gas as adsorbate. IR spectra were recorded with a Bruker Tensor 27 instrument equipped with a CsI splitting beam and a DTGS detector. Spectra were recorded over the range 4000–450 cm^{-1} at a resolution of 4 cm^{-1} and 50 scans per measurement. Reflectance measurements were performed with an attenuated total reflection (ATR) module, using a single-rebound Ge crystal.

Electrochemical measurements were carried out with CR2032 two-electrode coin cells supplied by Hohsen Corp. Powdered pellets 13 mm in diameter were prepared by pressing around 10 mg of active material with acetylene black (15 wt.-%) in a stainless steel grid. The electrolyte, supplied by Merck, was 1 M anhydrous $LiPF_6$ in a 1:1 mixture of ethylene carbonate and dimethyl carbonate. Cells were assembled in an M-Braun glove-box. Cycling tests were performed with a McPile II (Biologic) potentiostat-galvanostat system operating under a galvanostatic regime.

Supporting Information (see also the footnote on the first page of this article): Figure S1 includes plots of the Williamson and Hall equation for various (*hkl*) reflections for samples S-800 (■), PEG-800 (○) and PMMA-800 (△). Adsorption/desorption isotherms of the PEG-400 sample are shown in Figure S2.

Acknowledgments

This work was supported by Spanish Centro de Investigación Científica y Tecnológica (CICYT) (project MAT2005-03069) and the Junta de Andalucía (group FQM 175).

[1] A. R. West, *Solid State Chemistry and its Applications*, Wiley, NY, **1985**.
[2] M. M. Thackeray, *Prog. Solid State Chem.* **1997**, *25*, 1–71.
[3] C. Sigala, D. Guyomard, A. Verbaere, Y. Piffard, M. Tournoux, *Solid State Ionics* **1995**, *81*, 167–170.
[4] T. Ozhuku, S. Takeda, M. Iwanaga, *J. Power Sources* **1999**, *81*, 90–94.
[5] Q. Zhong, A. Bonakdarpour, M. Zhang, Y. Gao, J. R. Dahn, *J. Electrochem. Soc.* **1997**, *144*, 205–213.
[6] Y. K. Sun, Y. S. Lee, M. Yoshio, K. Amine, *Electrochem. Solid-State Lett.* **2002**, *5*, A99–A102.
[7] J. H. Kim, S. T. Myung, C. S. Yoon, S. G. Kang, Y. K. Sun, *Chem. Mater.* **2004**, *16*, 906–914.
[8] J. C. Arrebola, A. Caballero, M. Cruz, L. Hernán, J. Morales, E. Rodríguez Castellón, *Adv. Funct. Mater.* **2006**, *16*, 1904–1912.
[9] Y. Talyosef, B. Markovski, R. Lavi, G. Salitra, D. Aurbach, D. Kovacheva, M. Gorova, E. Zhecheva, R. Stoyanova, *J. Electrochem. Soc.* **2007**, *154*, A682–A691.
[10] M. G. Lazarraga, L. Pascual, H. Gadjov, D. Kovacheva, K. Petrov, J. M. Amarilla, R. M. Rojas, M. A. Martín-Luengo, J. M. Rojo, *J. Mater. Chem.* **2004**, *14*, 1640–1647.
[11] A. S. Aricò, P. G. Bruce, B. Scrosati, J. M. Tarascon, W. A. Schalkwijk, *Nat. Mater.* **2005**, *4*, 366–377.
[12] Y. Mosqueda, E. Pérez-Cappe, P. Aranda, E. Ruiz-Hitzky, *Eur. J. Inorg. Chem.* **2005**, *13*, 2698–2705.
[13] Y. Xia, M. Yoshio, H. Noguchi, *Electrochim. Acta* **2006**, *52*, 240–245.
[14] M. Sadakane, C. Takahashi, N. Kato, H. Ogihara, Y. Nodasaka, Y. Doi, Y. Hinatsu, W. Ueda, *Bull. Chem. Soc. Jpn.* **2007**, *80*, 677–685.
[15] G. Che, B. B. Lakshmi, E. R. Fisher, C. R. Martin, *Nature* **1998**, *393*, 346–349.
[16] J. Liu, Q. Wu, Y. Ding, *Cryst. Growth Des.* **2005**, *5*, 445–449.

[17] Z. Kang, E. Wang, M. Jiang, S. Liang, Y. Li, C. Hu, *Eur. J. Inorg. Chem.* **2003**, 370–376.
[18] X. R. Ye, D. Z. Jia, J. Q. Yu, X. Q. Xin, Z. Xue, *Adv. Mater.* **1999**, *11*, 941–942.
[19] A. Caballero, M. Cruz-Yusta, J. Morales, J. Santos-Peña, E. Rodríguez-Castellón, *Eur. J. Inorg. Chem.* **2006**, *9*, 1758–1764.
[20] A. Caballero, M. Cruz, L. Hernán, M. Melero, J. Morales, E. Rodríguez Castellón, *J. Power Sources* **2005**, *150*, 192–201.
[21] Y. Ein-Eli, J. T. Vaughey, M. M. Thackeray, S. Mukerjee, X. Q. Yang, J. McBreen, *J. Electrochem. Soc.* **1999**, *146*, 908–913.
[22] A. Strobel, S. Ibarra Palos, M. Anne, F. Le Cras, *J. Mater. Chem.* **2000**, *10*, 429–436.
[23] H. P. Klug, L. E. Alexander, *X-ray Diffraction Procedures for Polycrystalline and Amorphous Materials*, John Wiley & Sons, New York, **1974**.
[24] A. W. Rachinger, *J. Sci. Instrument.* **1948**, *25*, 254–255.
[25] J. Morales, J. L. Tirado, M. Macias, *J. Solid State Chem.* **1984**, *53*, 303–312.
[26] J. H. Kim, S. T. Myung, Y. K. Sun, *Electrochim. Acta* **2004**, *49*, 219–227.
[27] Z. Zhang, A. J. Rondinone, J. X. Ma, J. Shen, S. Dai, *Adv. Mater.* **2005**, *17*, 1415–1419.
[28] D. H. Park, S. T. Lim, S. J. Hwang, C. S. Yoon, Y. K. Sun, J. H. Choy, *Adv. Mater.* **2005**, *17*, 2834–2837.
[29] N. Li, C. J. Patrissi, G. Che, C. R. Martin, *J. Electrochem. Soc.* **2000**, *147*, 2044–2049.
[30] J. Huang, N. Matsunaga, K. Shimanoe, N. Yamazoe, T. Kunitake, *Chem. Mater.* **2005**, *17*, 3513–3518.
[31] R. S. Drago, in *Physical Methods in Chemistry*, W. B. Saunders Company, Philadelphia, **1977**, p. 176.
[32] P. R. Slater, *J. Fluorine Chem.* **2002**, *117*, 43–45.
[33] A. Manthiram, J. Kim, *Chem. Mater.* **1998**, *10*, 2895–2909.
[34] P. Arora, R. E. White, M. Doyle, *J. Electrochem. Soc.* **1998**, *145*, 3647–3667.
[35] A. Caballero, L. Hernán, M. Melero, J. Morales, M. Angulo, *J. Electrochem. Soc.* **2005**, *152*, A6–A12.
[36] K. Amine, H. Tukamoto, H. Yasuda, Y. Fujita, *J. Electrochem. Soc.* **1996**, *143*, 1607–1613.
[37] A. Caballero, L. Hernán, M. Melero, J. Morales, E. Rodríguez Castellón, *J. Electrochem. Soc.* **2005**, *152*, A552–A559.
[38] K. Ariyoshi, Y. Iwakoshi, N. Nakayama, T. Ohzuku, *J. Electrochem. Soc.* **2004**, *151*, A296–A303.
[39] Y. Terada, K. Yasaka, F. Nishikawa, T. Konishi, M. Yoshio, I. Nakai, *J. Solid State Chem.* **2001**, *156*, 286–291.

Received: February 1, 2008
Published Online: June 11, 2008

